



Experimental study of an oscillating water column wave energy converter based on regular waves

Soufiane EL Bouji¹ · Nouredine Kamil¹ · Zitouni Beidouri¹

Received: 19 April 2022 / Accepted: 9 October 2022 / Published online: 11 November 2022
© The Author(s), under exclusive licence to Sociedade Brasileira de Engenharia Naval 2022

Abstract

Increasingly, marine renewable energies are taking over as one of the most relevant solutions to minimize dependence on fossil fuels. The management and exploitation of such energy requires the optimization of converters that will, later on, ensure the conversion of hydraulic energy into electrical energy; among these converters are the oscillating water column. An OWC is characterized by its simplicity and its effectiveness against turbulent ocean conditions. The performance of OWCs depends strongly on the geometrical parameters of the air chamber such as: chamber walls, width, thickness of the front wall, slope at the bottom of the chamber and size of the opening. In this sense, the manuscript presents a parametric approach to investigate, by experimental tests, the hydrodynamic properties and the performance of oscillating water column wave energy converter (OWC). The effects of some geometrical key parameters of the system are analyzed. The tests are carried out on a small-size OWC. The work seems to be interesting in view of its experimental aspect. We have realized a prototype of an oscillating water column (OWC) which consists of a box (an air chamber) having the shape of parallelepipeds. The experimental results found by this study showed different optimums of: (a) the distance between the wave generator and the device (2 positions). (b) The depth of water in the hydraulic channel. (c) The immersion depth of the front wall of the chamber. (d) The opening at the bottom of the prototype. The results obtained show that the coupling of the geometrical parameters of the device and the conditions of installation leads to an improvement of the hydrodynamic performances of the OWC. The study also shows that the various optimums found give a considerable increase in the energy output.

Keywords Oscillating water column · Wave energy converter · Optimization

1 Introduction

The exploitation of energy from ocean waves is a challenge that progressively attracts the interest of researchers thanks to the significant energy potential available in the seas. In order to take advantage of this immense potential, several devices are patented as energy converters. Among these converters are the oscillating water columns (OWCs) which

have shown significant efficiency against the turbulent states of the oceans. In most cases, the OWC consists of a partially emerged chamber with an opening that includes an air turbine. Its operating principle is to generate pressure due to wave action, which alternately compresses and expands the trapped air, which—in return—is forced to flow through the air chamber into a turbine coupled to a generator acting as a PTO (power take-off). General reviews on the OWC cited in references [1–8] for turbines specific references can be found in [9–13], a review by [14] cited an important summary on the hydrodynamic performance of wave energy converters, including fundamental understandings on numerical modeling, physics and techniques for these wave energy converters.

OWC's hydrodynamic performance is mainly influenced by the converter's ability to extract hydraulic energy and convert it into pneumatic energy. While this performance factor is linked to the geometric parameters of the different components of the converter, climatic conditions

✉ Soufiane EL Bouji
soufiane1992jatel@gmail.com

Nouredine Kamil
nouredine.kamil@univh2c.ma

Zitouni Beidouri
Zitouni.beidouri@univh2c.ma

¹ Laboratory of Mechanics, Production and Industrial Engineering, LMPGI, Higher School of Technology of Casablanca, ESTC, Hassan II University of Casablanca, B.P. 8112, Oasis, Casablanca, Morocco

remain an important issue in the optimization of energy extraction. In fact, to characterize this connection, several researchers have proven the existence of an input between the dimensions and the location of the air chamber with the power absorbed at the PTO level. We can conclude that the change in a parameter related to the geometry of the OWC device attaches considerable optimization of energy standpoint [15].

The geometric parameters of the air chamber; namely the chamber walls, width, thickness of the frontal wall, slope at the bottom of the chamber, and size of the opening; were the subject of numerous investigations. Morris-Thomas et al. [16] examined experimentally the effect of frontal wall geometry on the efficiency of an OWC; they concluded that a curved wall was more effective than the rectangular one. Sheng [17] showed that the rearward curved duct has the best hydrodynamic performance as the forward curved duct especially for wave periods between 5 and 10. In the same direction, Dizadji and Sajadian [18] proved a dependence between the geometry of the chamber and the properties of the incident waves. The numerical study developed by [19] showed the effect of geometric parameters on the hydrodynamic performance of a U-shaped OWC. The results found by this search initially indicate an increase of η_{\max} and P_{\max} (denote the amplitudes of the free-surface elevation and the air pressure inside the chamber, respectively) then a decrease depending on the width of the vertical duct for the high frequency region. Deng et al. [20] also address the effects of wall-front dimensions. Çelik and Altun-kaynak [21] have also studied the effect of the various opening heights on the fluctuation of the free surface of OWC, this research [21] shows a linear relationship between the captured wave ratio and the transmitted wave heights.

In this paper, we have produced a prototype of an oscillating water column (OWC) which consists of a caisson (air chamber) in the form of parallelepipeds. Our novelty in this work will be a combination of experimental study between the geometric parameters of the air chamber and the OWC installation conditions to determine the different hydrodynamic performances.

As a first step, we will present the equations that govern the calculation of the powers absorbed by the OWC or the average incident power during a test period, this calculation of power will subsequently allow evaluating the performance of this device.

In a second step, we will present all the necessary materials for such an experiment specifying the method chosen for the experimental approach.

The exploitation of the results will be summarized by means of tables and graphs in terms of power for each variation of the geometric quantities.

In order to reach our main objective, we will evaluate the efficiency of our converter taking advantage of the values of the optimal powers for all the variations of the previous quantities.

1.1 OWC's primary output

The efficiency of an OWC is determined by the capacity of converting from wave energy to the so-called pneumatic energy. In general, the efficiency of such a device is defined by the power available to the turbines in relation to the power supplied to the system by the incident waves. This efficiency is illustrated below by the relationship:

$$\eta = \frac{\text{total energy absorbed}}{\text{total incident energy}} = \frac{P_{\text{OWC}}}{P_{\text{W}}} \quad (1)$$

where P_{OWC} the average power absorbed by the OWC given by the relation:

$$P_{\text{OWC}} = \frac{1}{T} \int_0^T PQ \, dt \quad (2)$$

With P the pressure of the area inside OWC measured by a manometer during a test, time T and Q the volume flow rate through the turbine.

The total power P_{W} of the incident wave averaged over a wave period can be solved using the equation:

$$P_{\text{W}} = E_{\text{W}} C_g \quad (3)$$

With E_{W} , the wave energy density is the amount of energy that is transported in a horizontal wave front region, perpendicular to the direction of the wave, which is given by the equation:

$$E_{\text{W}} = \frac{1}{2} \rho g b A^2 \quad (4)$$

$$C_g = \frac{1}{2} \frac{\Omega}{k} \left(1 + \frac{2kh}{\sinh(2kh)} \right) \quad (5)$$

With ρ the density of the water, g the gravitational acceleration, b the width of the part perpendicular to the direction of the incident waves of an OWC, A the amplitude of the waves and Ω the angular frequency which can be related with K the wave number by the following dispersion expressions:

$$\Omega^2 = gk \tanh(kh) \quad (6)$$



Fig. 1 The air chamber

2 Method and materials

The operating principle of OWC is to generate pressure due to the action of the incidental waves, which alternately causes a compression, then an expansion of the trapped air. The latter is forced to circulate via the air chamber in a

turbine coupled to a generator playing the role of a power take-off. In this sense, the design of the air chamber is necessary for the measurement of the pneumatic energy supplied by the OWC (Fig. 1).

In order to carry out the various experimental tests, a hydraulic flow channel is available, (Fig. 2). The channel is made up of five segments of Plexiglas (width: 10 m, height: 0.30 m and length: 0.30 m), a tank: (width: 0.705 m, height: 0.905 m. and length: 2 m), a centrifugal pump with a maximum flow rate of 3500 l/min and an analogue volumetric meter.

To avoid disturbances due to wave reflections an inclined plane was fixed upstream of the hydraulic channel (Fig. 3):

The wave generating system is powered by a 105 W motor with a maximum speed of 2000 tr/min and a speed variator. This mechanism is coupled to a square beater attached to the channel's bottom by an axis that allows back and forth movement (Fig. 4).

To obtain the corresponding values for each characteristic of the wave we use:

Fig. 2 The hydraulic channel

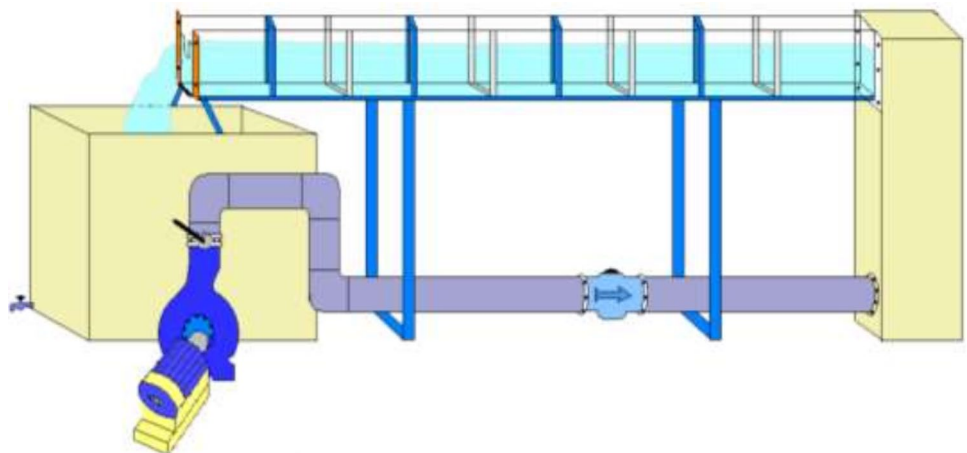


Fig. 3 Inclined plane

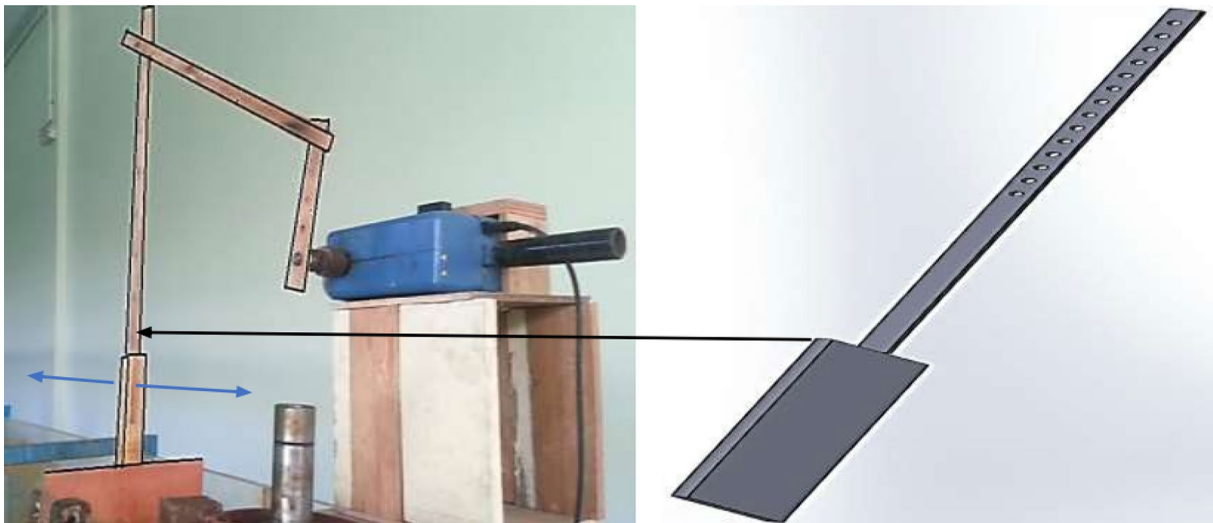


Fig. 4 The wave generating system

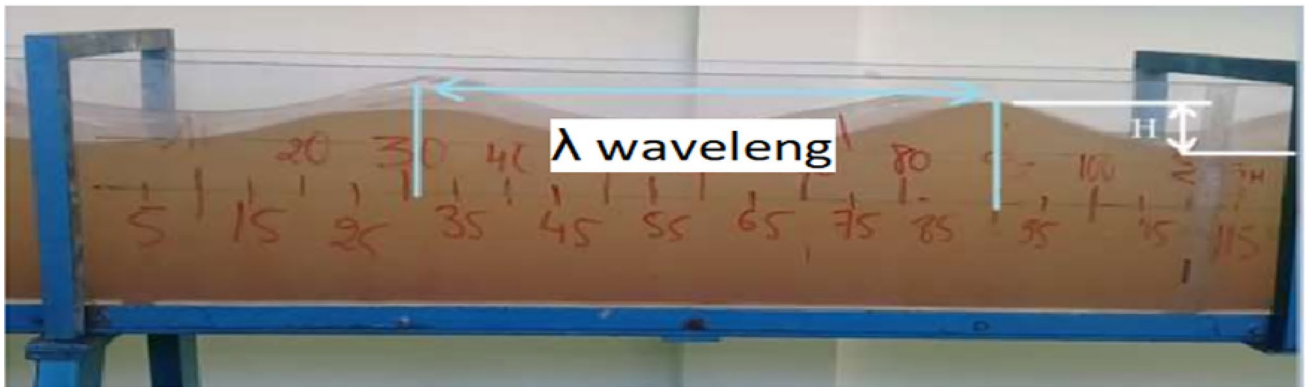


Fig. 5 Measure the length and height of the wave

Table 1 The characteristics of waves as a function of motor speed

Depth (cm)	w (rpm)	V (m/s)	λ (cm)	T (s)	H (cm)	A (cm)
$D = 18$ cm	62.5	0.182292	225	1.432	0.7	0.35
	80	0.233333	160	1.161	0.9	0.45
	102.5	0.298958	95	0.828	2	1
	125	0.364583	70	0.732	3.5	1.75
	157.5	0.459375	55	0.557	4.5	2.25
	190	0.554167	35	0.466	3.5	1.75
$D = 20$ cm	245	0.714583	27	0.366	2.5	1.25
	62.5	0.182292	235	1.608	3.3	1.65
	80	0.233333	162	1.28	2.9	1.45
	102.5	0.298958	120	1.008	4	2
	125	0.364583	95	0.848	4.5	2.25
	157.5	0.459375	68	0.521	7.1	3.55
$D = 23$ cm	190	0.554167	55	0.52	6.5	3.25
	245	0.714583	0.49	3.7	1.85	0
	45	0.13125	268	2.6	1	0.5
	62.5	0.182292	213	1.37	1.5	0.75
	80	0.233333	165	1.216	1.9	0.95
	102.5	0.298958	132	0.8655	3.1	1.55
	125	0.364583	122	0.8145	5	2.5
	157.5	0.459375	70	0.617	5.8	2.9
	190	0.554167	45	0.5665	6.5	3.25
	245	0.714583	40	0.436	3	1.5



Fig. 6 The geometry of the OWC in the hydraulic channel

- A chronometer: to determine the period of the generated wave (the time it takes for a wave to leave a peak point and return to the same point) We take time of ten successive waves for good accuracy.
- A camera: to take pictures to measure the length and height of the wave (Fig. 5).

The design of the chamber is necessary for the measurement of the pneumatic energy supplied by this device. It is a box in the form of a parallelepiped with an opening

through which water enters and an opening at the top through which an airflow exits to a turbine, from which the passage of energy mechanical to electrical energy is necessary (Fig. 6).

The anemometer is used to measure the air speed of the air chamber each time the water depth in the hydraulic column is changed as well as when the speed of the wave generator motor is varied. The following results are obtained (Table 1):

Table 2 Calculation of wave power

Depth (cm)	w (rpm)	ω	k	E_w (J)	C_g	P_w (Kw/m)
$D=23$ cm	45	2.416615	2.344478	0.061313	0.095137	0.005833
	62.5	4.586277	2.949859	0.137953	0.094522	0.01304
	80	5.167105	3.808	0.221338	0.136886	0.030298
	102.5	7.259619	4.76	0.589213	0.196542	0.115805
	125	7.71418	5.150164	1.532813	0.313549	0.480611
	157.5	10.18347	8.976	2.062553	0.423739	0.873985
	190	11.09126	13.96267	2.590453	0.511715	1.325574
	245	14.41101	15.708	0.551813	0.278942	0.153924
$D=20$ cm	62.5	3.907463	2.673702	0.667693	0.22037	0.147139
	80	4.90875	3.878519	0.515638	0.222901	0.114936
	102.5	6.233333	5.236	0.981	0.320225	0.31414
	125	7.409434	6.613895	1.241578	0.371962	0.46182
	157.5	12.05988	9.24	3.090763	0.412542	1.27507
	190	12.08308	11.424	2.590453	0.437555	1.133466
$D=18$ cm	245	12.82286	15.708	0.839368	0.361646	0.303554
	62.5	4.387709	2.792533	0.030043	0.043694	0.001313
	80	5.411886	3.927	0.049663	0.064012	0.003179
	102.5	7.588406	6.613895	0.24525	0.16903	0.041455
	125	8.583607	8.976	0.751078	0.33675	0.252925
	157.5	11.28043	11.424	1.241578	0.379221	0.470833
	190	13.48326	17.952	0.751078	0.360275	0.270595
245	17.16721	23.27111	0.383203	0.270296	0.103578	

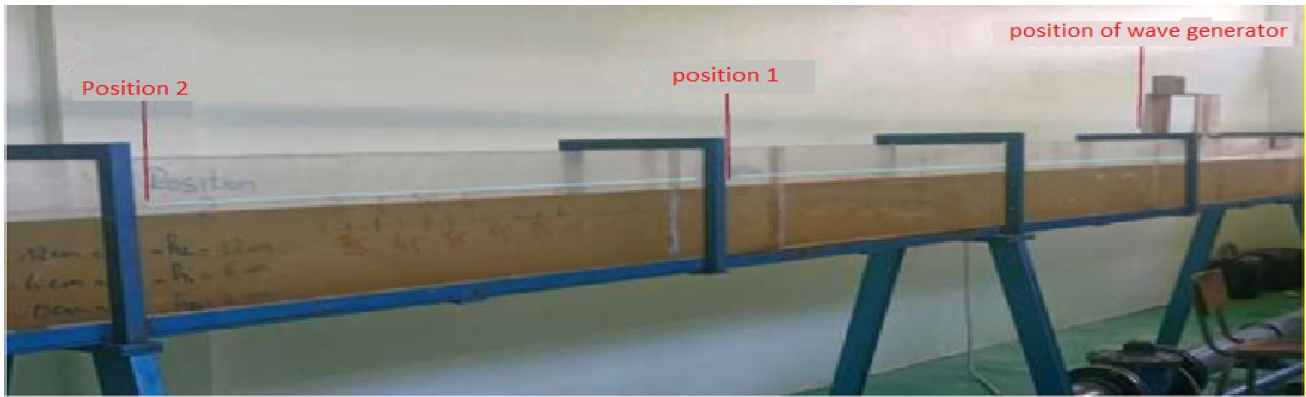


Fig. 7 Positions of the device

With: w and v the motor speed, λ wavelength, T period, H wave height, $A = H/2$ the amplitude, and D the water depth. Based on the results found and the equations quoted in the literature section, we can calculate the different wave characteristics for each water depth (Table 2):

In the following tests, several parameters are played with:

- The distance between the wave generator and the device for two positions (see Fig. 7).
- The depth of the water in the hydraulic channel noted D .
- The immersion depth of the front wall of the chamber noted d .
- The opening at the bottom of the prototype.

Table 3 The operating conditions: water depth of $D = 18$ cm, air chamber opening = 5 cm and orifice diameter = 1 cm

Water depth	Depth prototype	Position 1			Position 2			P_w (Kw/m)
		w (tr/min)	V_{air} (m/s)	P_{owc} (w)	w (tr/min)	V_{air} (m/s)	P_{owc} (w)	
$D = 18$ cm	$d = 0$ cm	62.5	0.29	2.3078402	62.5	0	0	0.001313
		80	0.41	3.2628103	80	0.75	5.9685705	0.003179
		102.5	0.62	4.9340127	102.5	0.66	5.2523378	0.041455
		125	0.69	5.4910818	125	0.6	4.7748502	0.252925
		157.5	0.4	3.1832294	157.5	0.45	3.5811341	0.470833
		190	0	0	190	0	0	0.270595
	$d = 6$ cm	245	0	0	245	0	0	0.103578
		62.5	0	0	62.5	0	0	0.001313
		80	0.74	5.888989	80	0.5	3.9790391	0.003179
		102.5	0.61	4.8544315	102.5	0.59	4.695269	0.041455
		125	0.7	5.5706632	125	0.7	5.5706632	0.252925
		157.5	0.55	4.3769445	157.5	0.57	4.5361067	0.470833
	$d = 12$ cm	190	0	0	190	0.21	1.6711942	0.270595
		245	0	0	245	0	0	0.103578
		62.5	0	0	62.5	0	0	0.001313
		80	0.66	5.2523378	80	0.53	4.2177823	0.003179
		102.5	0.77	6.1277336	102.5	0.62	4.9340127	0.041455
		125	0.88	7.0031322	125	0.85	6.7643868	0.252925
		157.5	1.01	8.0376983	157.5	1.15	9.1518524	0.470833
		190	0.62	4.9340127	190	0.61	4.8544315	0.270595
		245	0	0	245	0	0	0.103578

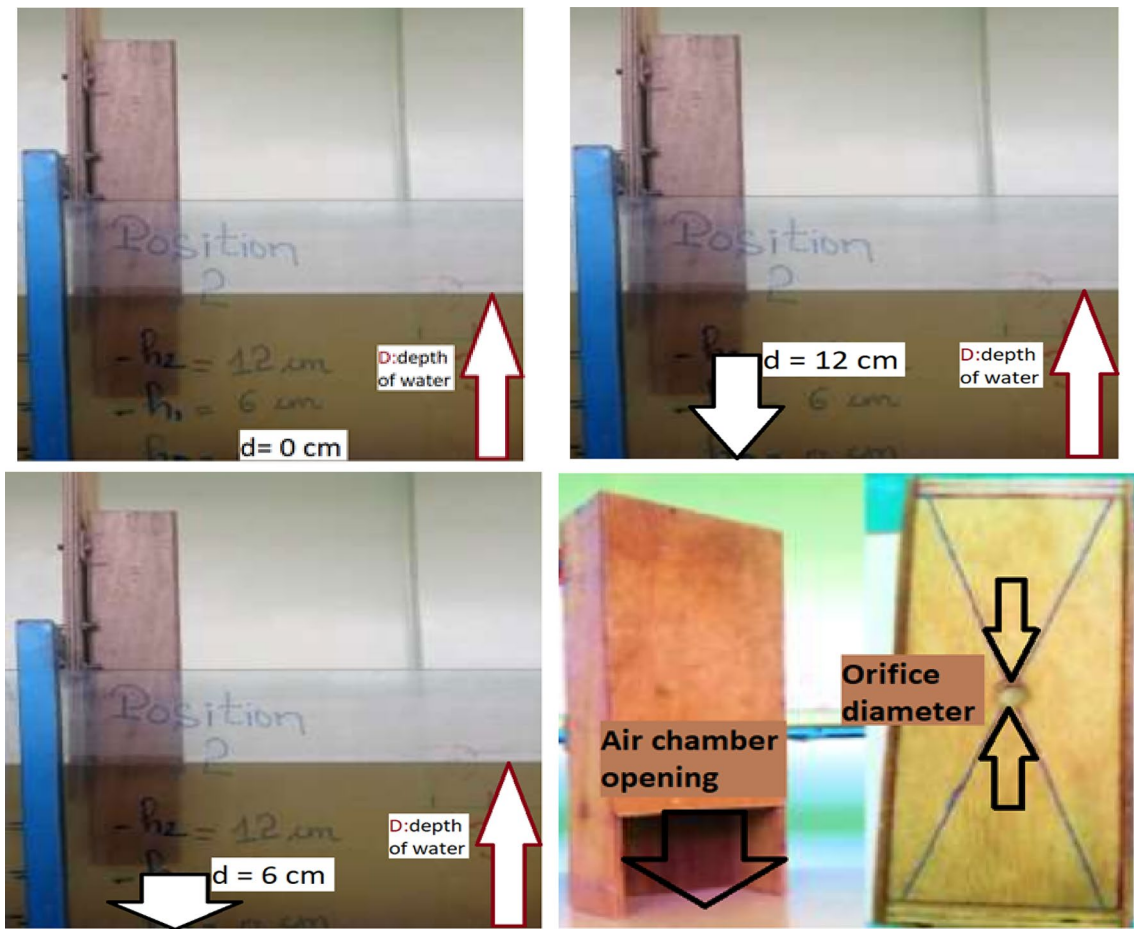


Fig. 8 All the experimental parameters under discussion

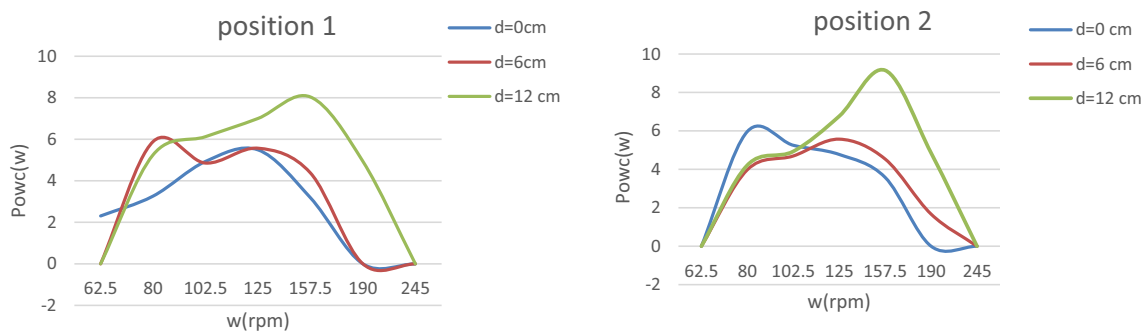


Fig. 9 The results obtained for the two positions at $D = 18$ cm

3 Result and discussion

We set ourselves in a water depth of $D = 18$ cm, where the operating conditions for the chamber are: Air chamber opening = 5 cm and Orifice diameter = 1 cm (Table 3), Fig. 8 describe all the experimental parameters under discussion.

The results obtained shown in the following Fig. 9 for the two positions at $D = 18$ cm, indicate that the immersion depth of the front wall of the chamber of the prototype influences the power available in the OWC. When the prototype is placed at a depth of 12 cm, it can be seen that higher powers are obtained at depths of 0 cm and 6 cm. This is due to the energy losses by friction of the particles with the soil of

Table 4 The operating conditions: water depth of $D = 20$ cm, air chamber opening = 5 cm and orifice diameter = 1 cm

Water depth	Depth prototype	Position 1			Position 2			P_w (Kw/m)
		w (tr/min)	V_{air} (m/s)	P_{owc} (w)	w (tr/min)	V_{air} (m/s)	P_{owc} (w)	
$D=20$ cm	$d=0$ cm	62.5	0	0	62.5	0.68	5.4115	0.147139
		80	0.57	4.536107	80	0.74	5.888989	0.114936
		102.5	0.72	5.729826	102.5	0.95	7.560206	0.31414
		125	0.97	7.71937	125	0.73	5.809408	0.46182
		157.5	0.42	3.342391	157.5	0.37	2.944487	1.27507
		190	0	0	190	0	0	1.133466
	$d=6$ cm	245	0	0	245	0	0	0.303554
		62.5	0	0	62.5	0.34	2.705744	0.147139
		80	2.59E-05	2.626163	80	0.45	3.581134	0.114936
		102.5	0.75	5.96857	102.5	0.73	5.809408	0.31414
		125	0.78	6.207315	125	0.82	6.525642	0.46182
		157.5	3.46E-05	3.501553	157.5	0.53	4.217782	1.27507
	$d=12$ cm	190	0	0	190	0	0	1.133466
		245	0	0	245	0	0	0.303554
		62.5	0	0	62.5	0.3	2.387421	0.147139
		80	3.46E-05	3.501553	80	0.36	2.864906	0.114936
		102.5	0.73	5.809408	102.5	0.45	3.581134	0.31414
		125	0.89	7.082714	125	0.92	7.32146	0.46182
	157.5	6.44E-05	6.525642	157.5	0.78	6.207315	1.27507	
	190	4.56E-05	4.615688	190	0.37	2.944487	1.133466	
	245	2.36E-05	2.387421	245	0	0	0.303554	

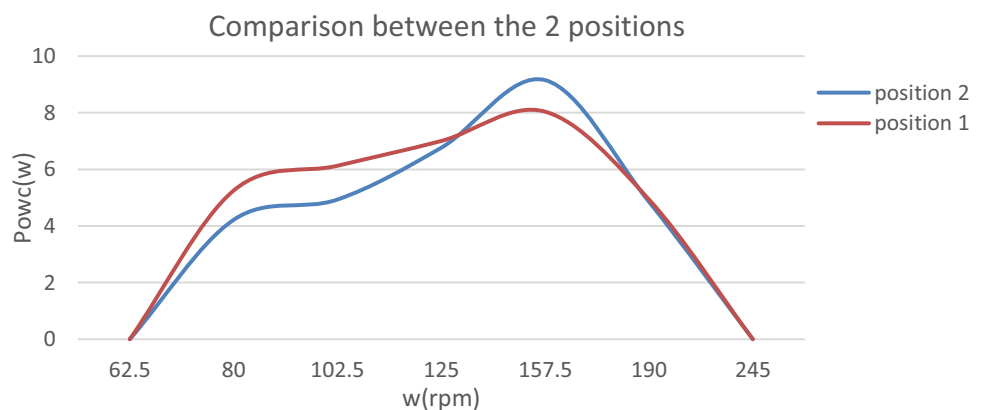
the hydraulic channel for deep media. When the prototype is placed in a shallow medium closer to the free surface where the friction is approximately low and the oscillations are high, more pneumatic energy is generated.

In order to determine the best operating environment of the device, we compare between the speeds where the powers are maximum for all the test (see Fig. 10). The maximum power generated during the tests in position 2 is higher than in position 1 (obtained for the immersion depth of the front wall of the chamber = 12 cm).

During the tests when the prototype is fixed in position 1, which is the closest to the wave generator, we notice

that there is a reflection of the waves arriving at the prototype through its wall. This has a direct influence on the characteristics of the wave and its energy potential; therefore; an impact on the pneumatic energy. This confirms the description of the wave energy distribution in an OWC in Fig. 10. We proceed in the same way for the 18 cm depth. Now we fix the water depth $D=20$ cm with the same operating conditions (Opening of the air chamber = 5 cm and the diameter of the orifice = 1 cm) (Table 4).

Using the data from the tests in a water depth $D=20$ cm, Fig. 11 is plotted for the 2 positions. It can be seen that for average water depths, the available power is better when the

Fig. 10 Comparison between the 2 positions at $D = 18$ cm

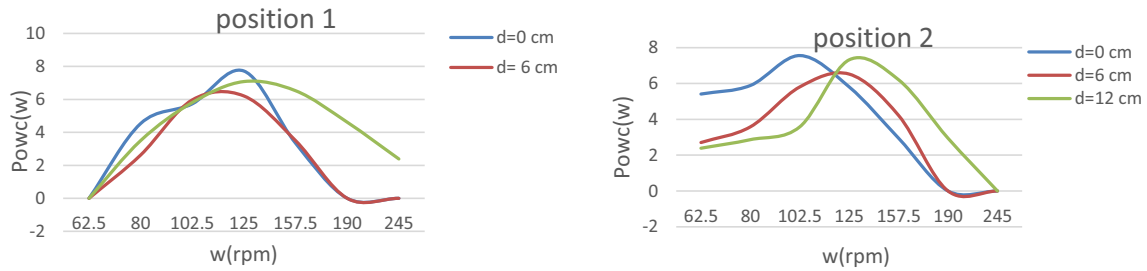


Fig. 11 The results obtained for the two positions at $D = 20$ cm

device is placed at the bottom of these depths (prototype depth = 0 cm), which is completely different from the results obtained in $D = 18$ cm. For the pattern representing the depth of the prototype = 12 cm. It can be observed that the different speeds of the wave generator (between 62.5 and 245 rpm) lead to considerable powers (see Table 5) which is not true for the other two patterns. This high speed of the particles leads to friction and therefore loss of kinetic energy in the air chamber (pneumatic energy).

The two figures in Fig. 12 represent a prototype depth = 0 cm. If we neglect the friction losses in this case,

the explanation of the maximum values of the powers can be linked to the oscillations of the water inside the air chamber, which reach a maximum height of water, leading to a very important air compression, thus a high airflow. This time, the maximum power corresponding to position 1 is higher than that of position 2, but it is important to note that for low speeds of the wave generator in this position one can have a significant power.

The following table presents the results corresponding to a water depth is set to $D = 23$ cm.

Table 5 The operating conditions: water depth of $D = 23$ cm, air chamber opening = 5 cm and orifice diameter = 1 cm

Water depth	Depth prototype	Position 1			Position 2			P_w (Kw/m)
		w (tr/min)	V_{air} (m/s)	P_{owc} (w)	w (tr/min)	V_{air} (m/s)	P_{owc} (w)	
$D = 23$ cm	$d = 0$ cm	45	0	0	45	0	0	0.005833
		62.5	0.48	3.819877	62.5	0.37	2.944487	0.01304
		80	0.835	6.645014	80	0.99	7.878534	0.030298
		102.5	0.7	5.570663	102.5	0.9	7.162296	0.115805
		125	0.91	7.241878	125	0.87	6.92355	0.480611
		157.5	0.49	3.899458	157.5	0.36	2.864906	0.873985
		190	0	0	190	0	0	1.325574
	$d = 6$ cm	245	0	0	245	0	0	0.153924
		45	0	0	45	0	0	0.005833
		62.5	0	0	62.5	0.26	2.069098	0.01304
		80	0.52	4.138201	80	0.74	5.888989	0.030298
		102.5	0.62	4.934013	102.5	0.8	6.366478	0.115805
		125	0.84	6.684805	125	0.87	6.92355	0.480611
		157.5	0.56	4.456526	157.5	0.61	4.854431	0.873985
	$d = 12$ cm	190	0	0	190	0.23	1.830356	1.325574
		245	0	0	245	0	0	0.153924
		45	0	0	45	0	0	0.005833
		62.5	0.36	2.864906	62.5	0.33	2.626163	0.01304
		80	0.54	4.297363	80	0.48	3.819877	0.030298
		102.5	0.79	6.286897	102.5	0.94	7.480624	0.115805
		125	0.76	6.048152	125	0.75	5.96857	0.480611
		157.5	0.81	6.44606	157.5	0.73	5.809408	0.873985
		190	0.36	2.864906	190	0.26	2.069098	1.325574
	245	0	0	245	0	0	0.153924	

Fig. 12 Comparison between the 2 positions at $D = 20$ cm

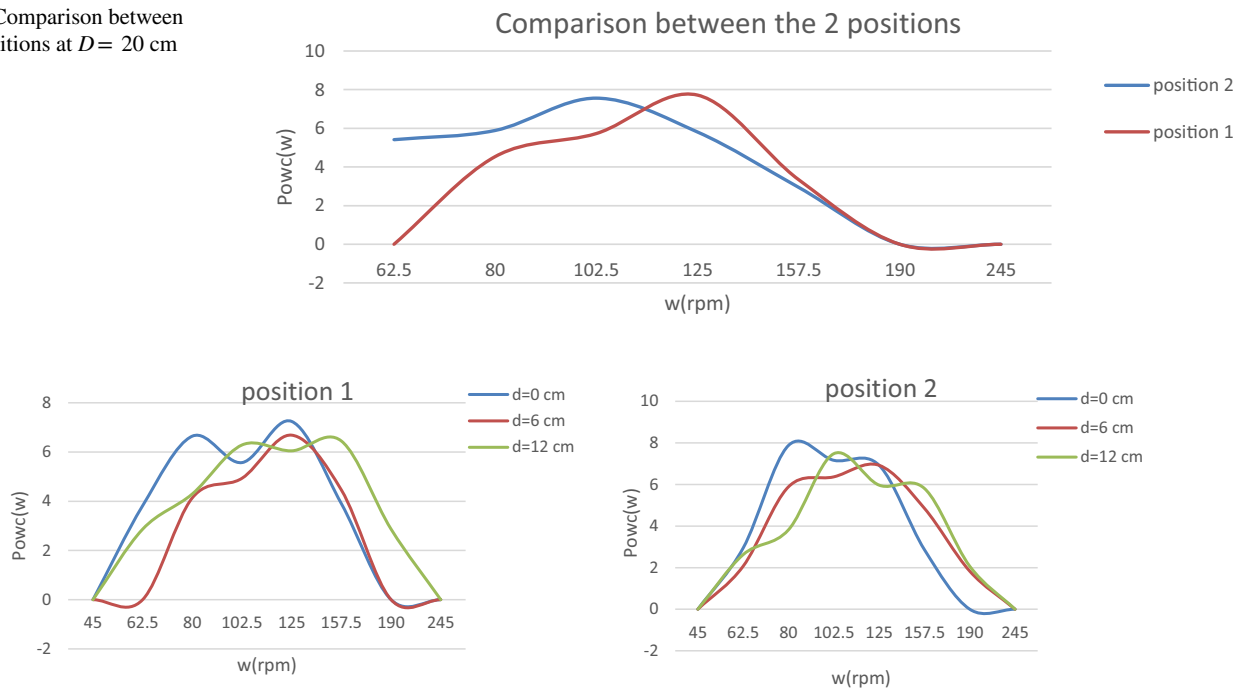
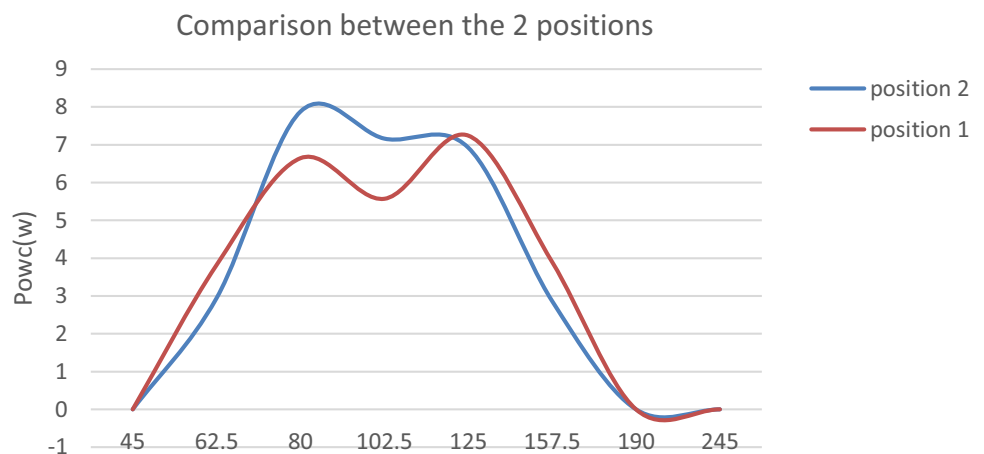


Fig. 13 The results obtained for the two positions at $D = 23$ cm

Fig. 14 Comparison between the 2 positions at $D = 23$ cm



The graphs show the variation of power in relation to W (rpm) in tow position for position 1 and position 2. The results for the different depths are confirmed, and the observations mentioned above are valid. We notice that in a depth of the prototype equal to 0 cm where the prototype is sunk to the bottom of the hydraulic channel the power is maximum, and zero for the last speeds. It is important to note that almost all the depths d achieve maximum power values at speeds between 80 and 157.5 rpm (Fig. 13).

Figure 14 represents the powers available in the OWC device for a depth of the prototype equal to 0 cm. Position 2 gives much better powers than position 1. This is due to reflection losses from the incident waves as position 1 is

closer to the wave generator. It can also be seen that for the last speeds the powers are zero; this could be due to the energy losses by particle friction, and the low amplitudes of the waves.

Referring to the results acquired previously, we can see that in order to be able to exploit the OWC device and produce significant power, the OWC must be fixed deeper in a medium or deeper environment (its position in relation to the sea or water level in our case). Because of the oscillations that can move inside the air chamber in a large volume that would subsequently allow for significant compression, and therefore a very large airflow. If we return to the case where the depth is low ($D = 18$ cm), we fall into a paradox from

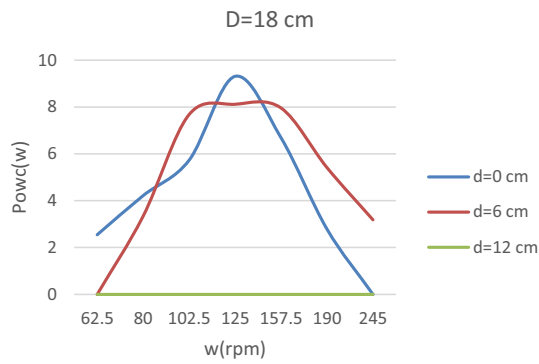


Fig. 15 The results obtained for $D = 18$ cm and air chamber opening = 11 cm

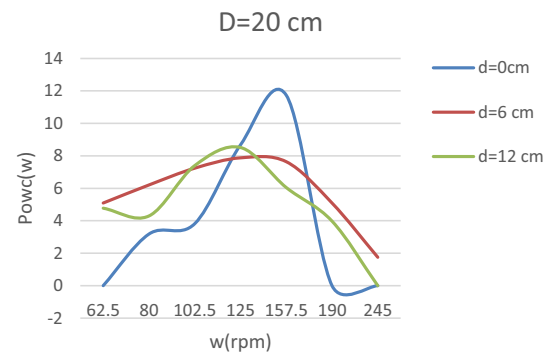


Fig. 16 The results obtained for $D = 20$ cm and air chamber opening = 11 cm

Table 6 The operating conditions: water depth of $D = 18$ cm, air chamber opening = 11 cm

Water depth	Depth prototype	Position 2		
		w (tr/min)	V_{air} (m/s)	P_{owc} (w)
$D = 18$ cm	$d = 0$ cm	62.5	0.32	2.546583
		80	0.53	4.217782
		102.5	0.72	5.729826
		125	1.17	9.311018
		157.5	0.84	6.684805
		190	0.35	2.785325
		245	0	0
	$d = 6$ cm	62.5	0	0
		80	0.42	3.342391
		102.5	0.965	7.679579
		125	1.02	8.117281
		157.5	1	7.958116
		190	0.68	5.4115
		245	0.4	3.183229
	$d = 12$ cm	62.5	0	0
		80	0	0
		102.5	0	0
		125	0	0
157.5		0	0	
190		0	0	
245		0	0	

Table 7 The operating conditions: water depth of $D = 18$ cm and Air chamber opening = 11 cm

Water depth	Depth prototype	Position 2		
		w (tr/min)	V_{air} (m/s)	P_{owc} (w)
$D = 20$ cm	$d = 0$ cm	62.5	0	0
		80	0.4	3.183229
		102.5	0.48	3.819877
		125	1.09	8.674357
		157.5	1.475	11.73831
		190	0	0
		245	0	0
	$d = 6$ cm	62.5	0.64	5.093175
		80	0.78	6.207315
		102.5	0.91	7.241878
		125	0.99	7.878534
		157.5	0.96	7.639788
		190	0.64	5.093175
		245	0.22	1.750775
	$d = 12$ cm	62.5	0.6	4.77485
		80	0.54	4.297363
		102.5	0.93	7.401042
		125	1.07	8.515192
157.5		0.76	6.048152	
190		0.5	3.979039	
245		0	0	

which we obtain better powers only this time the prototype is not fixed deep (depth of the prototype = 12 cm); whereas for a depth of the prototype equal to 0 cm the powers generated are not very important because of the losses by friction of the particles by the walls of the channel.

It is, therefore, necessary to avoid the areas where the phenomenon of wave reflection exists. From the above, we conclude that most of the results are given by the position 2 of the prototype so we will continue our studies only on this position.

Additionally, we will change another parameter of device. We will make an opening of 11 cm following the same procedure:

It can be seen that when the prototype is placed in a depth of 12 cm ($D = 18$ cm) (Table 6 and Fig. 15), there is no air flow, which results in a glued pattern on the horizontal axis of the engine speed (zero power). This is due to the water level not reaching the air chamber because of the large opening (11 cm). In this case, the maximum powers are generated

Table 8 The operating conditions: water depth of $D = 18$ cm and air chamber opening = 11 cm

Water depth	Depth prototype	Position 2		
		w (tr/min)	V_{air} (m/s)	P_{owc} (w)
$D=23$ cm	$d=0$ cm	62.5	0.54	4.297363
		80	1.02	8.117281
		102.5	0.91	7.241878
		125	0.85	6.764387
		157.5	0.62	4.934013
		190	0	0
	$d=6$ cm	62.5	0.56	4.456526
		80	0.89	7.082714
		102.5	0.82	6.525642
		125	1.05	8.356027
		157.5	0.96	7.639788
		190	0.33	2.626163
	$d=12$ cm	62.5	0.39	3.103649
		80	0.48	3.819877
		102.5	0.75	5.96857
		125	1.225	9.748723
		157.5	1.615	12.85249
		190	1.15	9.151852
	245	0.47	3.740296	

for a prototype depth of 12 cm, which is compatible with the above results.

The maximum powers are given by a prototype depth of 12 cm (Table 7 and Fig. 16), which is completely different to the results of other tests seen previously. During the tests, and at the highest level of the device, it was noticed that the water does not cover the entire opening until the arrival of

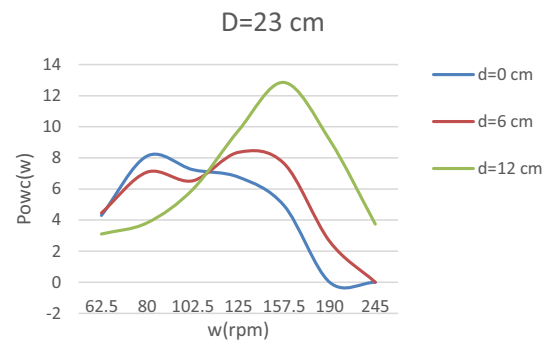


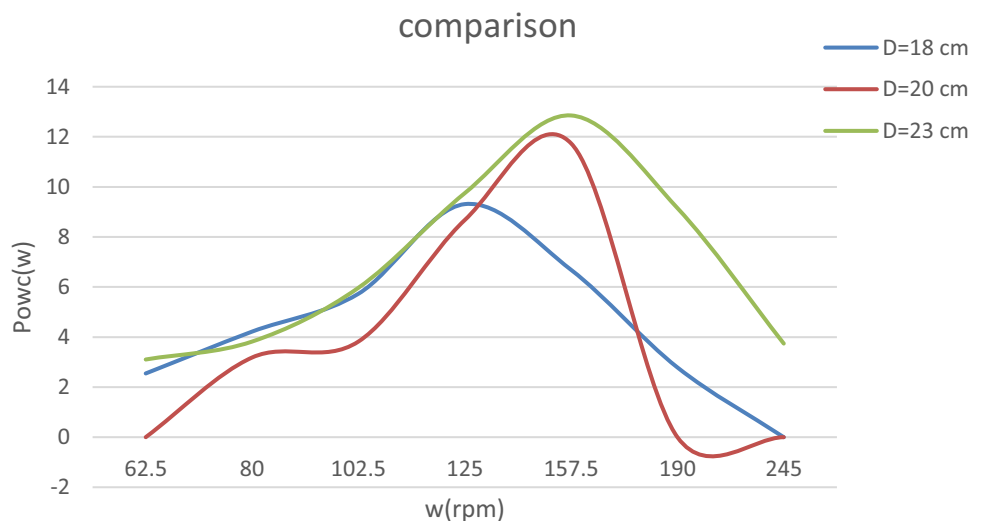
Fig. 17 The results obtained for $D = 23$ cm and air chamber opening = 11 cm

the wave crests, which subsequently causes a quantity of atmospheric air to enter with the water, and therefore a significant compression, thus explaining of the results obtained.

The graphs (Table 8 and Fig. 17) represent powers that are larger than the results for other water depths, whether for a 5 cm or 11 cm opening. The explanations in the graph for the 20 cm water depth (11 cm opening) are also valid in this case.

If we compare the three maximum powers available in the OWC device of the three water depths ($D = 18, 20, 23$ cm) (Fig. 18), we notice that the one of the water depth 23 cm and the prototype 12 cm is the most important. As already explained, when the air chamber opening has been changed and when it is fixed at the highest level, there is an entrainment of atmospheric air with the incoming water in the device, which—in return—gives an additive amount of energy (more compression than the air in the air chamber alone).

Fig. 18 Comparison between the three maximum powers available in the OWC device of the three water depths ($D = 18, 20, 23$ cm)



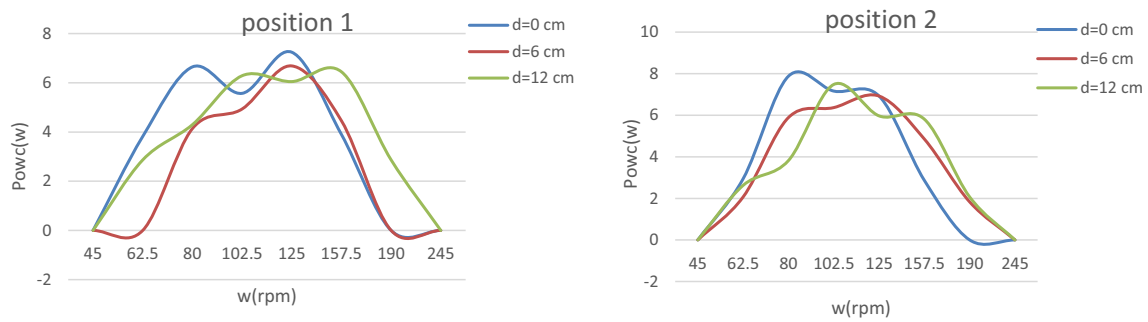


Fig. 19 The efficiency for a water depth $D=18$ cm of the first opening

3.1 Efficiency of the first opening

The effectiveness of the device is a challenge that must always be raised. In order to evaluate any kind of optimization, the dependence between geometric quantities and performance has been approved by several authors such as: Bouali and Larbi [22] who reported that the maximum efficiency of OWC at the frontal wall is related to the depth of submersion with $0.45 h$ (where h is the depth of water). The same authors in [23] also showed a performance gain about 7% obtained for three optimal parameters. This study also shows that there is a unique triplet (T, h, H) that makes the device more efficient. In the same sense [18] have conceptualized several chamber geometries in order to examine their efficiency. On the one hand, the results have shown a dependence between the chamber geometry and the properties of

the incident waves. On the other hand, the optimal geometry examined with this study is 32% in efficiency term.

Figure 19 represents the efficiency for a water depth $D=18$ cm for the two positions and for the different depths of the prototypes. The maximum efficiency can be generated by the prototype at this depth is 37.5%. It is given by a wave power $P_w=0.244$ W knowing that this power is the smallest among all the other wave powers. This translates to the fact that the efficiency of OWC depends strongly on the conditions of the sites chosen for the installation. In fact, to generate more energy in an area with a low wave power, it is recommended to install the chamber with a depth very close to the free water surface.

Although there is not much drop in power for the depth of $D=20$ cm (Fig. 20), it has a very low efficiency which does not exceed 0.4% due to the high power generated by the waves during the tests. Even with this very low efficiency

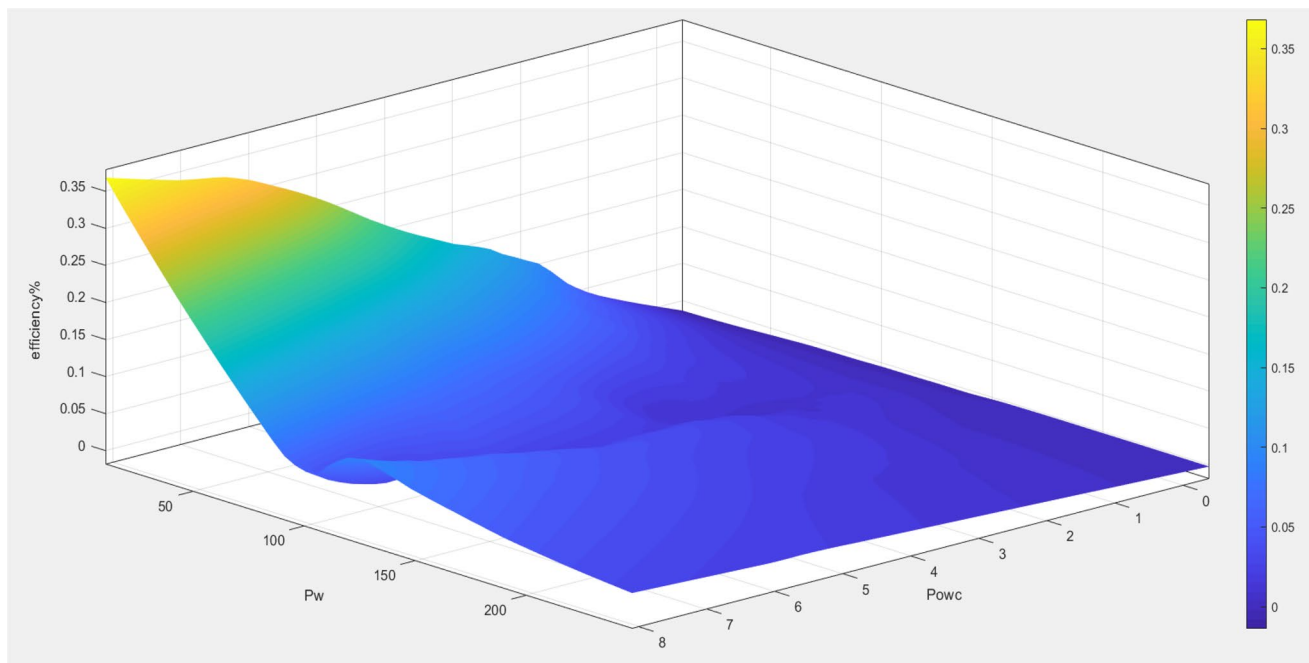


Fig. 20 The efficiency for a water depth $D=20$ cm of the first opening

result, it is not possible to judge the benefit of OWC since it can generate more power compared to the depth of $D = 18$ cm.

For the water depth $D = 23$ cm (Fig. 21), the maximum efficiency does not exceed 8% which is also low for the depth of $D = 18$ cm. But the system response in terms of power for this depth is still relevant among all other depths and this choice of depth may be the optimal choice despite the low efficiency of OWC.

3.2 Efficiency of the second opening

In the previous paragraph, we have seen the effect of variation of depth D on the efficiency of the converter for a constant opening. Then we will present the effect of variation of opening on the efficiency of the device.

For the second opening, it can be seen that the maximum efficiency generated is 38.12% with an increase of 1% compared to the first opening for the same depth of $D = 18$ cm (Fig. 22). But again, it can be seen that this efficiency will be cancelled out for a prototype depth of $d = 0$ cm. This is due to the level of the water not reaching the air chamber because of the opening becoming large (11 cm). Therefore, it can be proposed that for shallow water depths it is recommended to work with such small openings in order to take advantage of the maximum pneumatic energy.

At a depth of $D = 20$ cm, the efficiency is still very low which agrees with the other results found (Fig. 23). In fact, the maximum efficiency generated at this depth does not exceed 0.6% with an increase of 0.2% compared to the

other opening. This decrease in efficiency is due to the high power generated with the wave generator.

The maximum efficiency generated at a depth of $D = 23$ cm is about 12% with an increase of 4% (Fig. 24). This is also low compared to $D = 18$ cm to the same aperture. However, this decrease in efficiency is still due to the high power of the waves generated during the tests.

4 Use of goodness-of-fit statistics in this study

We examine the goodness-of-fit statistics in order to visualize the quality of fit. The Curve Fitting tool of the MATLAB software supports these goodness-of-fit statistics for parametric models:

4.1 Sum of squares due to error SSE

This statistic calculates the overall deviation of the response values from the response values' fit. It is frequently abbreviated as SSE and is known as the summed square of residuals:

$$SSE = \sum_{i=1}^n w_i (y_i - \hat{y}_i)^2$$

The fit will be more accurate for prediction if the value is closer to 0, which means that the model has a smaller random error component.

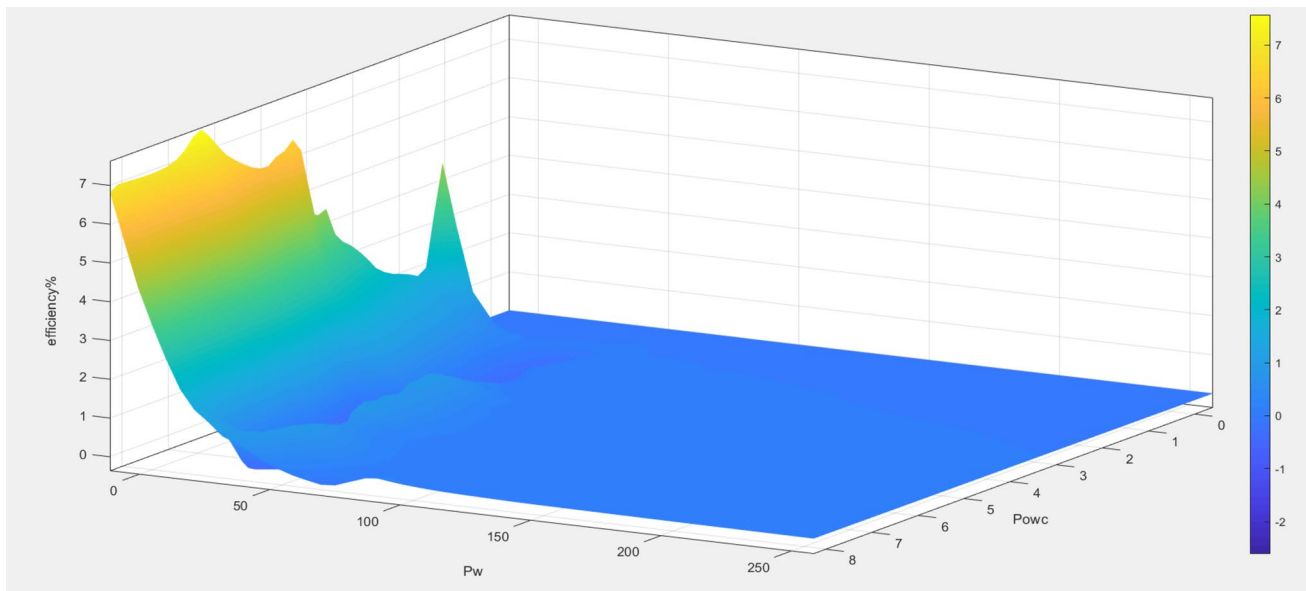


Fig. 21 The efficiency for a water depth $D = 23$ cm of the first opening

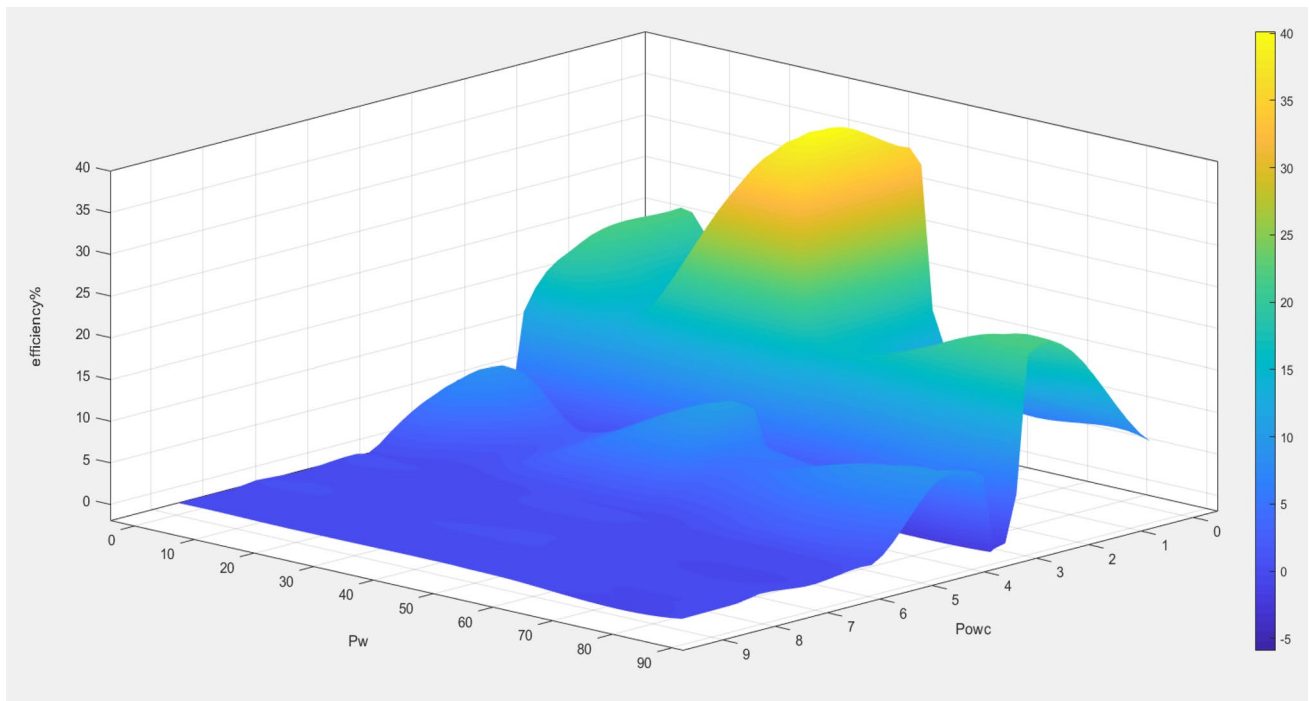


Fig. 22 The efficiency for a water depth $D = 18$ cm of the second opening

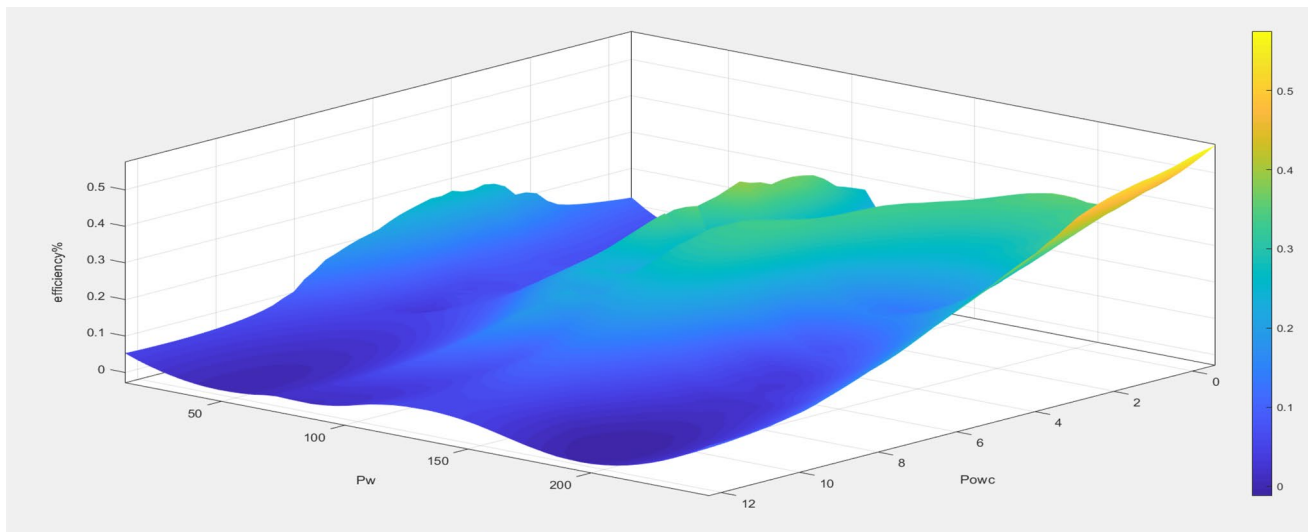


Fig. 23 The efficiency for a water depth $D = 20$ cm of the second opening

4.2 The mean square error MSE

The mean square error or the residual mean square MSE is defined as:

$$MSE = \frac{SSE}{\nu}$$

ν denotes the number of independent pieces of information concerning the n data points needed to compute the sum of squares.

Identical to SSE, an MSE value closer to 0 denotes a fit that is more useful for prediction.

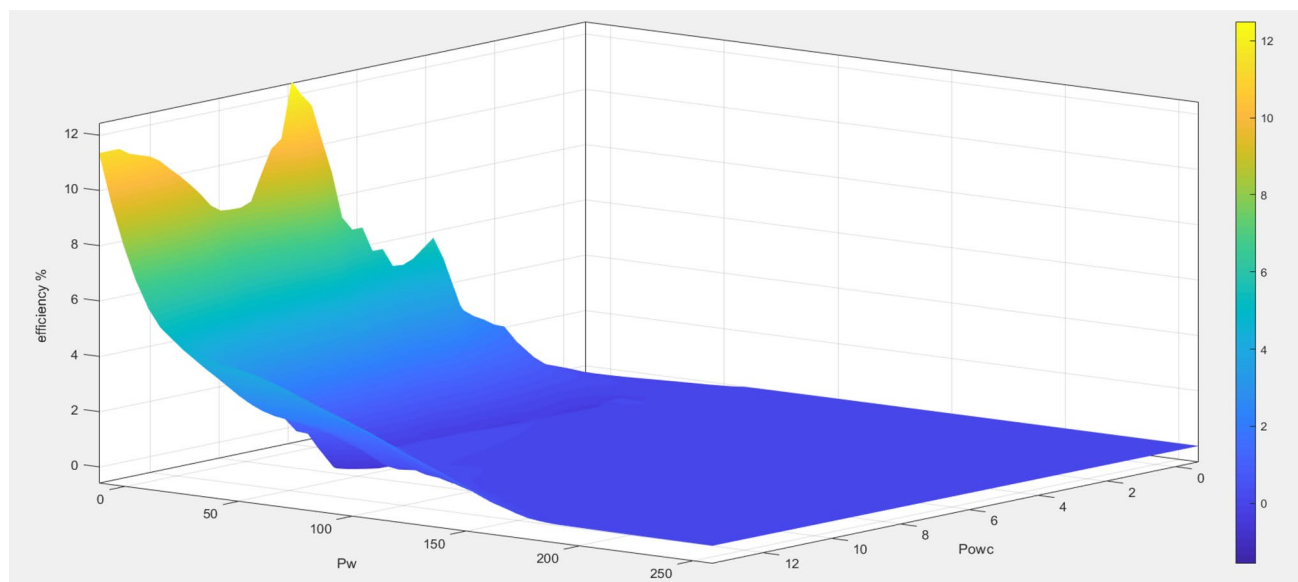


Fig. 24 The efficiency for a water depth $D = 23$ cm of the second opening

5 Conclusion

OWC's power response proved the existence of an optimal relationship between geometric quantities and converter efficiency. The experimental results found by this study showed the different optimum of:

- The distance between the wave generator and the device (2 positions).
- The depth of water in the hydraulic channel.
- The immersion depth of the front wall of the chamber.
- The opening at the bottom of the prototype.

Moreover, make it possible to size the OWC.

For the depth of water in the hydraulic channel noted D , we can confirm a rather direct correlation between the absorbed power and the depth D . This correlation is no longer valid when we approach the free surface of water (depth $d = 12$ cm).

These results can be explained by the losses due to the friction of the particles with the channel walls as well as the reflection of the waves.

We have also concluded that the installation of the OWC at a level very near to the free surface causes a quantity of atmospheric air to enter the chamber, which can contribute to an additional quantity of energy.

The comparison between the two positions (1 and 2) shows that most of the maximum power is given by the second position.

For the response of OWC in terms of efficiency, it was shown that the efficiency increases with the decrease of the

water depth D and increases with the increase of the prototype depth d . This is due to the decrease of the power arriving to the prototype, which can subsequently decrease the friction between the water particles and the oscillations, thus generating more pneumatic energy.

For the effect of the opening of the prototype, we can observe a significant increase either in terms of power or in terms of efficiency. Provided that we avoid areas where the depth of water and prototype is small, in our case the power was zero for the couple ($D = 18$ cm, $d = 0$ cm), an increase of 4% of efficiency was generated for a depth of $D = 23$ cm with the second opening = 11 cm. Therefore, we can conclude that the opening is an important factor that should be taken into account when designing OWC in order to take maximum advantage of it.

It is very important to note that the power response is the most compatible to describe the efficiency of OWC because of the low values calculated by the efficiency. This difference in compatibility between the two responses is due to the high power generated by the waves during their movement and also the effect of the different random characteristics of the waves such as the reflection phenomenon of the waves.

References

1. J. Falnes, A review of wave-energy extraction. *Mar. Struct.* **20**(4), 185–201 (2007). <https://doi.org/10.1016/j.marstruc.2007.09.001>
2. B. Drew, A.R. Plummer, M.N. Sahinkaya, A review of wave energy converter technology. *Proc. Inst. Mech. Eng. Part J. Power Energy* **223**(8), 887–902 (2009). <https://doi.org/10.1243/09576509JPE782>

3. A.F. de O. Falcão, Wave energy utilization: a review of the technologies. *Renew. Sustain. Energy Rev.* **14**(3), 899–918 (2010). <https://doi.org/10.1016/j.rser.2009.11.003>
4. T.V. Heath, A review of oscillating water columns. *Philos. Trans. R. Soc. Math. Phys. Eng. Sci.* **370**(1959), 235–245 (2012). <https://doi.org/10.1098/rsta.2011.0164>
5. I. López, J. Andreu, S. Ceballos, I. Martínez de Alegría, I. Kortabarria, Review of wave energy technologies and the necessary power-equipment. *Renew. Sustain. Energy Rev.* **27**, 413–434 (2013). <https://doi.org/10.1016/j.rser.2013.07.009>
6. A. Muetze, J.G. Vining, Ocean wave energy conversion—a survey, in *Conference Record of the 2006 IEEE Industry Applications Conference Forty-First IAS Annual Meeting*, October, vol. 3 (2006), pp. 1410–1417. <https://doi.org/10.1109/IAS.2006.256715>
7. M. Shalby, D.G. Dorrell, P. Walker, A. Elhanafi, An experimental investigation into the wave power extraction of a small-scale fixed multi-chamber OWC device, in *2019 IEEE Energy Conversion Congress and Exposition (ECCE)*, September (2019), pp. 4982–4987. <https://doi.org/10.1109/ECCE.2019.8912191>
8. N. Delmonte, D. Barater, F. Giuliani, P. Cova, G. Buticchi, Review of oscillating water column converters. *IEEE Trans. Ind. Appl.* **52**(2), 1698–1710 (2016). <https://doi.org/10.1109/TIA.2015.2490629>
9. N. Ansarifard, S.S. Kianejad, A. Fleming, A. Henderson, S. Chai, Design optimization of a purely radial turbine for operation in the inhalation mode of an oscillating water column. *Renew. Energy* **152**, 540–556 (2020). <https://doi.org/10.1016/j.renene.2020.01.084>
10. T. Setoguchi, S. Santhakumar, H. Maeda, M. Takao, K. Kaneko, A review of impulse turbines for wave energy conversion. *Renew. Energy* **23**(2), 261–292 (2001). [https://doi.org/10.1016/S0960-1481\(00\)00175-0](https://doi.org/10.1016/S0960-1481(00)00175-0)
11. T. Setoguchi, M. Takao, Current status of self rectifying air turbines for wave energy conversion. *Energy Convers. Manag.* **47**(15), 2382–2396 (2006). <https://doi.org/10.1016/j.enconman.2005.11.013>
12. D.L. O’Sullivan, A.W. Lewis, Generator selection and comparative performance in offshore oscillating water column ocean wave energy converters. *IEEE Trans. Energy Convers.* **26**(2), 603–614 (2011). <https://doi.org/10.1109/TEC.2010.2093527>
13. W. Sheng, A. Lewis, Power takeoff optimization to maximize wave energy conversions for oscillating water column devices. *IEEE J. Ocean. Eng.* **43**(1), 36–47 (2018). <https://doi.org/10.1109/JOE.2016.2644144>
14. W. Sheng, Wave energy conversion and hydrodynamics modelling technologies: a review. *Renew. Sustain. Energy Rev.* **109**, 482–498 (2019). <https://doi.org/10.1016/j.rser.2019.04.030>
15. S.E. Bouji, Z. Beidouri, N. Kamil, Design and optimization of an oscillating water column wave energy converter, in *2019 International Conference of Computer Science and Renewable Energies (ICCSRE)*, July (2019), pp. 1–3. <https://doi.org/10.1109/ICCSRE.2019.8807608>
16. M.T. Morris-Thomas, R.J. Irvin, K.P. Thiagarajan, An investigation into the hydrodynamic efficiency of an oscillating water column. *J. Offshore Mech. Arct. Eng.* **129**(4), 273–278 (2007). <https://doi.org/10.1115/1.2426992>
17. W. Sheng, Motion and performance of BBDB OWC wave energy converters: I, hydrodynamics. *Renew. Energy* **138**, 106–120 (2019). <https://doi.org/10.1016/j.renene.2019.01.016>
18. N. Dizadji, S.E. Sajadian, Modeling and optimization of the chamber of OWC system. *Energy* **36**(5), 2360–2366 (2011). <https://doi.org/10.1016/j.energy.2011.01.010>
19. D. Ning, B. Guo, R. Wang, T. Vyzikas, D. Greaves, Geometrical investigation of a U-shaped oscillating water column wave energy device. *Appl. Ocean Res.* **97**, 102105 (2020). <https://doi.org/10.1016/j.apor.2020.102105>
20. Z. Deng, L. Wang, X. Zhao, P. Wang, Wave power extraction by a nearshore oscillating water column converter with a surging lip-wall. *Renew. Energy* **146**, 662–674 (2020). <https://doi.org/10.1016/j.renene.2019.06.178>
21. A. Çelik, A. Altunkaynak, Experimental and analytical investigation on chamber water surface fluctuations and motion behaviours of water column type wave energy converter. *Ocean Eng.* **150**, 209–220 (2018). <https://doi.org/10.1016/j.oceaneng.2017.12.065>
22. B. Bouali, S. Larbi, Contribution to the geometry optimization of an oscillating water column wave energy converter. *Energy Procedia* **36**, 565–573 (2013). <https://doi.org/10.1016/j.egypro.2013.07.065>
23. B. Bouali, S. Larbi, Sequential optimization and performance prediction of an oscillating water column wave energy converter. *Ocean Eng.* **131**, 162–173 (2017). <https://doi.org/10.1016/j.oceaneng.2017.01.004>

Publisher's Note Springer Nature remains neutral with regard to jurisdictional claims in published maps and institutional affiliations.

Springer Nature or its licensor (e.g. a society or other partner) holds exclusive rights to this article under a publishing agreement with the author(s) or other rightsholder(s); author self-archiving of the accepted manuscript version of this article is solely governed by the terms of such publishing agreement and applicable law.